Effect of niobium variation on the properties of directed energy deposited CrCoNiCuNbx coatings

Ayo Alabi[1*], *Abimbola* Popoola[1], *Olawale* Popoola[2], and *Ntombi* Mathe[3]

[1]Chemical, Metallurgical and Materials Engineering, Faculty of Engineering and Built Environment, Tshwane University of Technology, P.M.B. X680, Pretoria, South Africa
[2]Center for Energy and Electric Power, Electrical Engineering, Faculty of Engineering and Built Environment, Tshwane University of Technology, P.M.B. X680, Pretoria, South Africa
[3]Photonic Center, Council for Scientific and Industrial Research, Pretoria, South Africa

Abstract. The presence of a refractory metal such as niobium in high-entropy alloys improves their hardness values, wear and corrosion resistance. Herein, a CrCoNiCuNbx alloy-system used as coating was developed by directed energy deposition technique, and the effect of niobium variation on microstructural and phase evolution, hardness, wear characteristics and corrosion resistance were studied in comparison to the base alloy (CrCoNiCu) and steel baseplate. In addition, structure-property correlations were conducted, and it was observed that the variation of niobium resulted in phase and microstructural evolutions of the alloy-system. These directly influenced the hardness, wear and corrosion resistance of coatings as it resulted in a 62.47% improvement in hardness at 0.50 niobium content and a more than 260-fold increase in corrosion resistance in 3.5% NaCl electrolyte at 0.25 niobium compared to the mild steel substrate. The wear resistance at 10 and 15 N applied loads for the coating with 0.75 niobium content were also found to be enhanced by about 93.94% and 80.83%, respectively, when compared to those of steel substrate.

1 Introduction

Steel remains the preferred engineering material for use in traction parts of most heavy-duty machines used in excavation, construction or tillage purposes. However, it is susceptible to wear and corrosion under most service conditions [1], [2]. In recent times, surface engineering has been utilized for the development of protective coatings as it enhances hardness as well as wear and corrosion resistance to protect the surface of the steel. A protective surface enhancement technique that has been widely explored is laser cladding, which is a well-known additive manufacturing (AM) coating technology [3, 4]. In addition, high-entropy alloys (HEAs) are relatively new alloying that has been considered for steel coatings due to their high corrosion and wear resistance with improved hardness profile. Their tunable and tailorable properties include (but are not limited to) remarkable combined

* Corresponding author: ayo.alabi@ymail.com

toughness and strength, excellent resistance to high temperature oxidation, high wear and corrosion resistance have made them attractive as coatings in many engineering application [5].

The wide range of possible elemental combinations that could result in potential low, medium or HEAs for engineering application have been classified based on the number of constituent elements present and their values of configurational entropies. High-entropy alloys have minimum of five elements combined in equiatomic or near equiatomic ratios with configurational entropy (ΔS_{conf}) > 1.5R, those with two elemental constituent and ΔS_{con} < 1R are classified as low-entropy alloys, while medium-entropy alloys fall into categories with 3 to 4 elements and 1R < ΔS_{con} < 1.5R, where R is the gas constant [6]. Reports have shown that most medium and HEAs (MHEAs) were derived from the quest to improve the properties of existing binary or ternary alloys. Along this line, CrCoNi alloy-system has been widely studied and several methods adopted to improve and tune its properties for applications that require excellent corrosion, wear and radiation resistance, remarkable fracture toughness at cryogenic temperature, high temperature oxidative stability and combined strength and ductility [7-9]. One of the several methods considered in improving the alloy's system properties is the addition of copper (Cu). Previous works showed that Cu addition to MHEAs has the tendency of promoting grain boundary liquid-solid separation that leads to micro-segregation before solidification due to the positive mixing enthalpy of Cu with other constituent elements [7]. This results in a two-phase composite structure with coordinate deformation profile that is beneficial in improving plasticity and strength of Cu-containing alloy-systems. In addition, nanoprecipitates of a Cu-rich secondary phase that is useful in restricting dislocation movements during deformation in Cu containing MHEAs have also been reported [11]. Ren, et al. [9] investigated the role of primary face centered cubic (FCC) CrCoNi-rich dendritic phase and well distributed secondary FCC Cu-rich inter-dendritic phase in enhancing the wear resistance of an arc melted equiatomic CoCrCoCu alloy. It was found that the inter-dendritic phase formed a compacted glaze layer on the worn surface during dry sliding, which subsequently improved the wear resistance of the alloy. However, the authors mentioned that the presence of the secondary phase reduced the hardness of the alloy due to the strength-ductility trade-off. In another study, Xie, et al. [8] investigated the effect of Cu addition on the properties of the widely studied FCC CrCoNi MEA. The Cu content was varied at 0.16, 0.33, 0.75 and 1.0 molar ratios. In addition, directed energy deposition (DED) technique was used to reduce the earlier reported liquid-solid separation associated with other fabrication methods which led to micro-segregation in CoCrNiCu alloy-system [7]. Micro-segregation was inhibited because of reduced diffusion time in the liquid phase associated with that fabrication method. An ultrafast cooling rate also resulted in microstructural refinement by enhancing nucleation rate and then slowing down crystal growth. The tensile strength and ductility of the alloy were improved from 140 to 820 MPa and 1 to 11% respectively, at optimum Cu content of 1 molar ratio.

Whenever improvement in hardness, wear, corrosion and high temperature oxidation resistance are required in MHEA-based coatings for surface protection purposes, the addition of refractory metals such as molybdenum and niobium (Nb) are applicable [12, 13]. Nb addition to HEA systems have been reportedly associated with the formation of Laves phases that improved hardness, wear and strength due to resistance to dislocation movements. Dispersion strengthening effect and formation of eutectic phases as a result of Nb addition have also been mentioned in previous work [5]. Tsau, et al. [14] observed variation in hardness values and good corrosion resistance of CrFeCoNiNbx alloy-system after the addition of Nb due to the formation of dual dendritic phases. By varying Nb, He, et al. [15] designed a eutectic CrCoFeNiNbx alloy-system and studied its mechanical properties, microstructural and phase evolution. The present study aims to develop CrCoNiCuNbx alloy-

system and investigate its phase and microstructural evolution, hardness, wear and corrosion resistance as a function of Nb variation. This is expected to further enhance the hardness value, wear and corrosion resistance of CrCoNiCu MEA alloy.

2 Methodology

2.1 Fabrication

Apart from Nb powder with D50 particle size, all powders used for the fabrication of the coatings were 99.9% pure and– 90 + 45 µm particle size was used. The coatings were fabricated in situ by adding 0.25, 0.50, 0.75 and 1.0 molar ratios of Nb content at a time to an equiatomic CrCoNiCu powder that was premixed in a tubular mixer for 10 hours and at 74 rpm. Clads with $Nb_{0.25}$CrCoNiCu, $Nb_{0.5}$CrCoNi, $Nb_{0.75}$CrCoNiCu and $Nb_{1.0}$CrCoNiCu HEA compositions were fabricated by the DED AM IPG fiber laser. Five overlapping clads were built on a 100 x 100 x 5 mm^3 steel baseplate. Clads were deposited on a single mild steel substrate using process parameters presented in Table 1.

Table 1: Process Parameters

Laser Power (W)	Scanning Speed (m/minute)	Carrier Gas Flow Rate (l/min)	Powder Feed Rate (g/min)	Beam Diameter (mm)	Track overlap (%)	Purge Gas Flow Rate (l/min)
1200	1.2	2.0	0.24	2.0	50	20

2.2 Metallography and characterization

The clads were cut, mounted and prepared according to ASTM E3 metallographical standard procedure. Thereafter samples were etched with mable reagent (4g of $CuSO_4$ + 20ml of 1M HCl + 20 ml of water) and their microstructures were examined using JEOL JSM-6010LAM Scanning Electron Microscope. PANalytical Empyrean x-ray diffraction equipment was used to determine the X-ray diffratograms of all samples at 20 mA, 40 KV and Cu-K alpha source. The hardness of the samples were determined using Zwick/Roell Indentec (ZHVµ) Vickers microhardness machine under 300 gram force load for adwell time of 10s and spacing of 100µm between indentations with an average of 10 indentations per sample. A TRB^3 Anton Paar Tribometer connected to a S 128 surtronic profilometer was used to conduct dry sliding wear tests on the coatings at room temperature using the ball-on-flat rotating configuration. A 6mm steel ball was used as a sliding counter body. The test was conducted under applied loads of10 and 15 N with 1000 sliding cycles per test. The coefficient of friction and the penetration depth of the steel ball were recorded by the attached surtronic profilometer. The corrosion resistance of the clads were analyzed from the tafel interpolation of their polarization curves as generated in a 3.5% NaCl electrolyte. The corrosion was conducted using Autolab® PGSTAT 302 that is computer controlled using NOVA software version 2.1.

3 Result and discussions

3.1 Microstructural characterization

The secondary and back scattered electron SEM images of clads were presented in Figures 1 and 2. The evident morphological changes observed in Figure 1a to 1e showed that Nb addition to CrCoNiCu resulted in a phase transformation. The transformation progressed as Nb addition increased in Figure 1b to 1e. The BSE images in Figure 2 are presented alongside their topographical images. Figure 2a revealed that the microstructure of CrCoNiCu was characterized by two FCC phases. EDS Elemental mapping and spot analyses showed that the dominant FCC1 phase was rich in Cr, Co, and Ni. A segregated Cu-rich (FCC2) phase was also observed, which was either partially or completely etched by the corrosive marble etchant, leaving behind partially or fully etched-Cu pits. The positive mixing enthalpy of Cu with Ni, Co and Cr (4, 6 and 12 KJ/mol) promoted its phase separation and segregation.A similar observation was reported by Xie, et al. [11] who fabricated CrCoNiCu alloy system by DED. Cai, et al. [16] also observed the etching of segregated Cu that led to the formation of pits in FeCoCrNiCu alloy fabricated by laser cladding method. Figure 2b shows the effect of 0.25 molar ratio Nb addition on the microstructural evolution of CrCoNiCuNbx HEA system. The microstructure was dominated by FCC1 phase with traces of Laves phase that was precipitated at the grain boundaries. It is noteworthy that the addition of Nb to CrCoNiCu promoted the emergence of HCP and growth of Laves phases. This can be attributed to the negative mixing enthalpy of Nb (– 24KJ/mol) that led to its preferential reaction with Cr, Co and Ni over Cu.

When Nb content was increased stepwisely from 0.25 to 1.0 molar ratio, a change in the morphology of the alloy system that corresponded to the transformation of the Laves phase precipitates into intergranular submicron-lamellar structures was observed, as shown in Figure 2e. The volume fraction of Nb-rich submicron-lamellar structures increased as the Nb content was increased. The alloy showed morphologies with marked imprints of plate-like dendritic structures with a network of high-volume fraction of Nb-rich Laves phases when Nb content of 0.75 and 1.0 molar was added. A similar observation was reported by Lu, et al. [17] that studied the effect of Nb variation on the microstructural evolution of CrCoNi MEA.

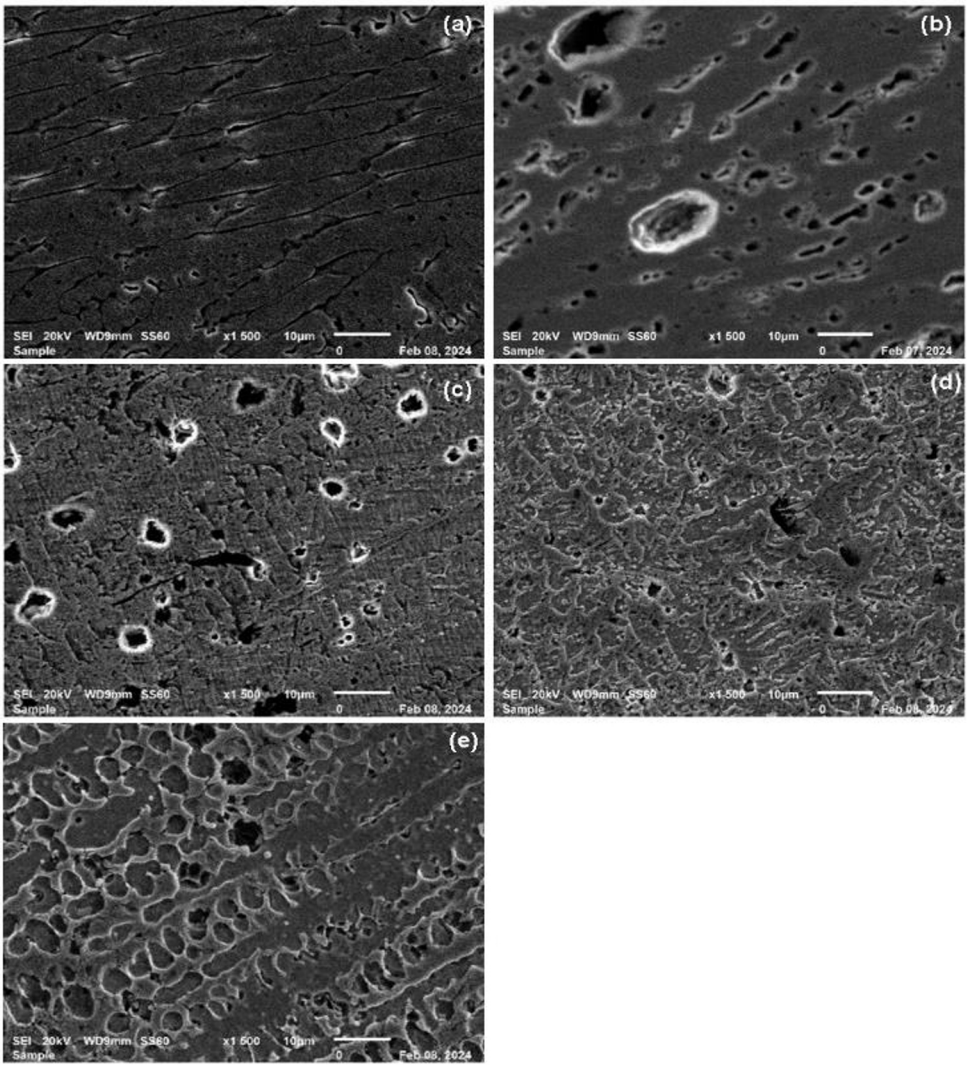

Fig. 1: SEM images of (a) CrCoNiCu (b) $CrCoNiCuNb_{0.25}$ (c) $CrCoNiCuNb_{0.50}$ (d) $CrCoNiCuNb_{0.75}$ (e) $CrCoNiCuNb_{1.0}$

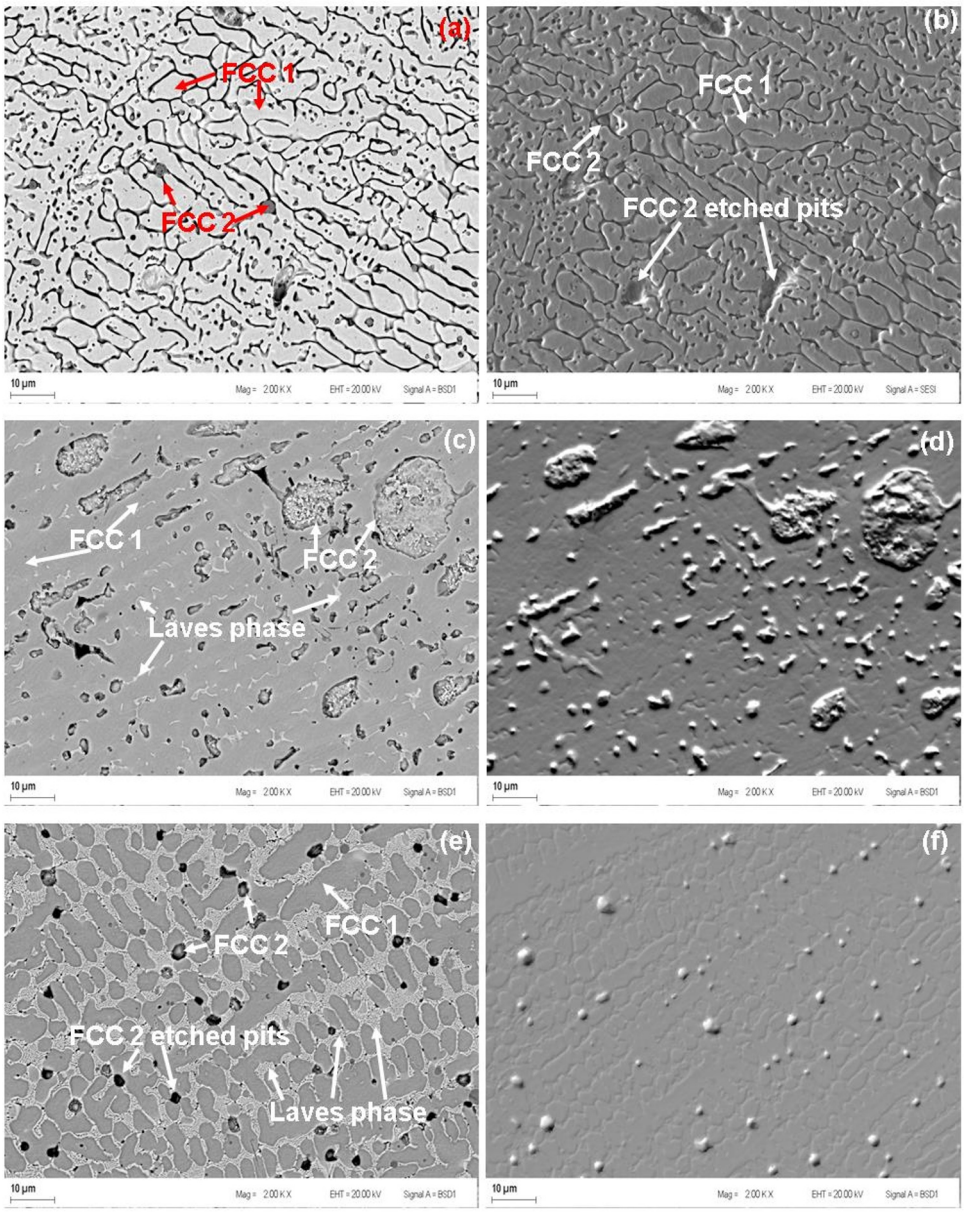

Fig. 2: BSE and topographic image of (a, b) CrCoNiCu (c, d) CrCoNiCuNb0.25 and (e, f) CrCoNiCuNb1.0

3.2 XRD phase identification

A HEA alloy-system was successfully developed, and the crystal structures of phases present in the alloy system were identified by XRD. The XRD patterns of CrCoNiCu and CrCoNiCuNbx alloy-systems are presented in Figure 3. The peaks confirmed the existence of two {FCC1 (CrCoNi) and FCC2 (Cu-rich} phases in CrCoNiCu alloy. FCC1 and FCC2 exhibited several stretched and almost overlapping minor peaks and major stretched and

overlapping peaks occurring at 43.16° in the 2θ regions. Corresponding to the dark granular and white intergranular phases shown in the SEM micrograph in Figure 1a. Adding Nb to CrCoNiCu resulted in the emergence of Cr(CoNi)Nb-type HCP Laves phases, which exhibited several overlapping peaks in the 2θ regions at different Nb content. At 0.25 Nb content, overlapping peaks of Laves phases were observed at the major diffraction peak intensity region stretching the peaks from 43.75 to 44.71° in the 2θ regions. Increasing the content of Nb also gradually decreased the diffraction peak intensity of the FCC phases and showed the emergence of more Laves phases peaks in the 2θ regions. This indicated that the addition of Nb to the alloy system was beneficial for phase transformation from FCC to Laves phase.

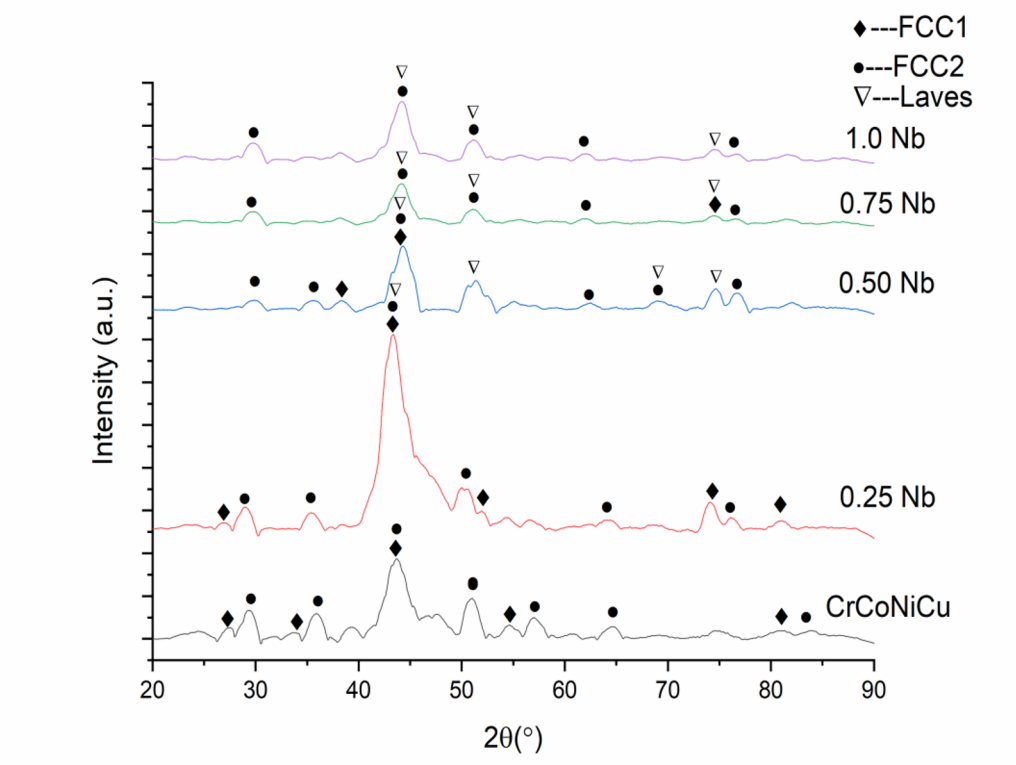

Fig. 3: XRD Patterns of As-clad CrCoNiCuNbx alloy-system (x=0.25, 0.50, 0.75 and 1.0)

3.3 Microhardness

SEM-EDS microstructures with XRD phase identification results revealed that CrCoNiCuNbx alloy-system was composed of soft FCC and hard HCP Laves phases. The hardness of the alloy-system was tested as Nb content was increased and hardness values were compared with those of mild steel baseplate and CrCoCuNi base alloy as shown in Figure 4. The CrCoCuNi and CrCoCuNiNbx alloy-system exhibited better hardness values than the steel baseplate. Furthermore, an optimal hardness value of 413.8 ± 10.38 $HV_{0.3}$ was recorded for CrCoCuNiNbx at 0.5 Nb addition and attributed to solid solution strengthening and dislocation movement restriction effect by FCC2 and Laves precipitates due to the transformation of FCC1 + FCC2 into FCC1 + FCC2 + Laves phases. The combination of these phases imparted excellent hardness to the alloy-system. The enhanced hardness value was an appreciable improvement over the 242 $HV_{0.2}$ of the DED CrCoNi alloy reported by

Deshmukh et al. [18]. Moreover, Ren et al. [9] reported a lower 179.2 $HV_{0.5}$ for as-cast arc melted CrCoNiCu alloy. A drop in hardness value observed between 0.5 and 0.75 Nb addition is attributable to the transformation of fine lamellar Laves phases into a more complex lamellar network that increased the brittleness of the alloy. Another drastic increase in microhardness occurred when Nb content was increased from 0.75 to 1.0. This was attributed to an increase in the volume fraction of hard Laves phases as Nb content was increased. Jiang, et al. [19] have earlier observed a similar trend in CoCrFeNbxNi HEA-system.

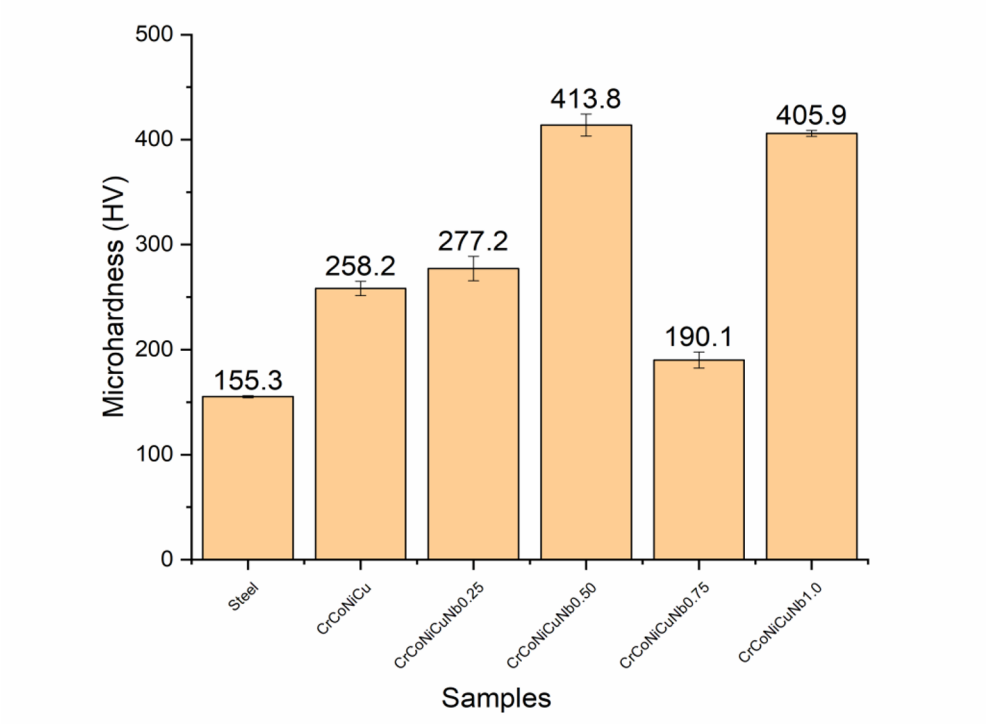

Fig. 4: Microhardness of As-clad CrCoNiCuNbx alloy-system (x=0.25, 0.50, 0.75 and 1.0) for repairs of worn steel part surfaces.

3.4 Tribological performance

Figures 5 (a) and (b) present the dry sliding coefficient of friction and wear rate of samples at 10 and 15 N applied load. The coefficient of friction of steel increased from 0.516 to 0.560 as the applied load increased from 10 to 15 N. In contrast, a decrease in the coefficient of friction with an increase in applied load was observed in CrCoNiCu and CrCoNiCuNbx alloy-systems. The coefficient of friction of alloys was lower when a higher applied load of 15 N was used and decreased stepwise as Nb content increased. However, at both 10 and 15 N applied load, a decrease by more than 90% coefficient of friction was observed at 1.0 Nb addition. This is attributable to higher frictional force that was associated with greater contact pressure which changed the mechanism of interaction and surface area between the sliding surfaces. The correlation between a low coefficient of friction and a high hardness value is well documented in the literature [20-22].

Likewise, the wear rate at both 10 and 15 N applied load decreased as Nb content was increased. This was because of the increase in volume fraction of a more orderly structured hard Nb-rich Laves phases as Nb content was increased, which enhanced the wear resistance of samples. Lower wear rates of the order $\times 10^{-5}$ mm^3/Nm were observed at 0.75 and 1.0 Nb addition for both 10 and 15 N applied load when compared with those of the order $\times 10^{-4}$ mm^3/Nm and $\times 10^{-3}$ mm^3/Nm observed in the mild steel substrate and CrCoNiCu, respectively. Significant improvement in the wear resistance of Nb-rich Laves phases containing high-entropy alloys due to enhanced hardness has been reported and was confirmed by Archard's wear law that relates material's hardness to its wear resistance [23]. However, a deviation from the law is possible as observed at 0.75 Nb content; and may be attributed to the formation of protective oxide film that separated the mating bodies, thereby reducing wear. Plastically deformed Cu-rich thin oxide layer that is reinforced by hard Laves phases can form compacted protective tribo-layer that hardens the alloy's subsurface, thereby hindering further sliding friction-induced damage [9, 24].

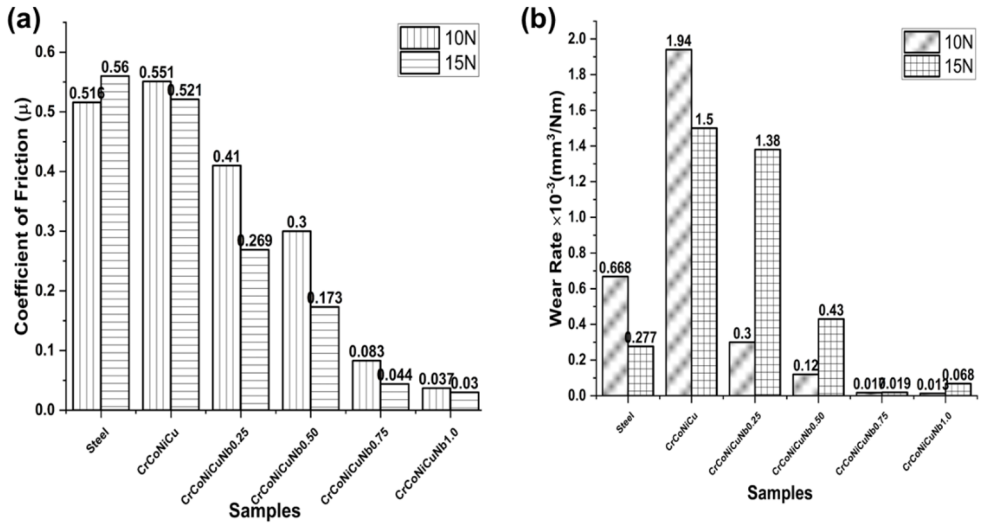

Fig. 5: Coefficient of friction and wear rate of samples.

3.5 Corrosion characteristics of samples

Figure 6 shows the potentiodynamic curves of all samples tested in a 3.5% NaCl electrolyte. The corrosion resistance of CoCrNiCu and CrCoNiCuNbx alloy-system-based coatings were compared with that of the mild steel baseplate. The evident similarity in polarization curves of samples indicated that they all exhibited spontaneous passivation and pseudo-passive characteristics in 3.5% NaCl electrolyte, without showing distinct active-passive transition. Tafel interpolated corrosion test data for all samples were also presented in Table 1. Generally, a more negative E_{corr} and lower j_{corr} signify better corrosion resistance. Although the alloy with 0.75 Nb content produced a more negative E_{corr}, the sample with 0.25 Nb addition produced the lowest j_{corr}. Consequently, it exhibited the highest polarization resistance and lowest corrosion rate in 3.5% NaCl, which translated to more than a 260-fold improvement in corrosion resistance than the steel baseplate. Apart from the sample with 0.75 Nb addition, all coatings showed better corrosion resistance than the steel baseplate.

According to Shi, et al. [25] HEAs with refined and ordered Laves phase-containing structures could result in a nobler trans-passive potentials and lower current densities than those with coarse structures. The assertion agrees with the findings as the alloy with 0.25 Nb addition exhibited optimum corrosion resistance and coarsening of lamellar structure became obvious at 0.75 Nb content.

Table 2: Extrapolated polarization data for CoCrNiCu and CrCoNiCuNbx alloy-system-based coatings tested in 3.5% sodium chloride electrolyte.

Samples	Corrosion Potential Ecorr (V)	Corrosion Current Density jcorr (A/cm^2)	Polarization Resistance (Ω)	Corrosion Rate (mm/year)
Steel	– 0.8148	7.21×10^{-5}	3451.2	0.8380
CrCoNiCu	– 0.9779	3.52×10^{-5}	1772.9	0.4092
$CrCoNiCuNb_{0.25}$	– 0.9895	2.76×10^{-5}	103680	0.0032
$CrCoNiCuNb_{0.50}$	– 0.8882	6.85×10^{-5}	1423.8	0.7964
$CrCoNiCuNb_{0.75}$	– 1.0609	9.21×10^{-5}	723.23	1.0704
$CrCoNiCuNb_{1.0}$	– 0.9303	4.03×10^{-5}	3483.8	0.4684

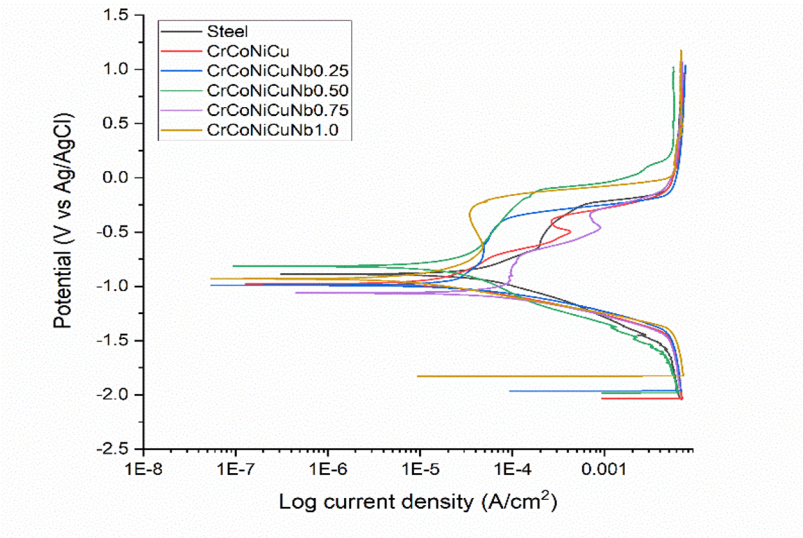

Fig. 6: Potentiodynamic polarization curves for samples.

4 Conclusion

This study successfully developed a CrCoNiCuNbx alloy-system that was coated on mild steel using the DED AM. The effect of Nb variation of the coatings on microstructural and

phase evolutions, microhardness values, wear characteristics and corrosion resistance were investigated, and the following conclusions were drawn based on the results obtained:

1. The secondary and backscattered SEM-EDS images revealed that the addition of Nb led to the emergence of HCP Laves phases from a dual FCC phased CrCoNiCu. The XRD analysis confirmed the presence of FCC1 and FCC2 in CrCoNiCu coating and the emergence of HCP Laves phases when Nb was added to the alloy-system.
2. The addition of Nb to CrCoNiCu resulted in an increase in hardness values due to solid solution strengthening and dislocation movement restriction by FCC2 and Laves phases dispersion effect. An optimum microhardness of 413.8 ± 10.38 $HV_{0.3}$ was exhibited by the $CoCrNiCuNb_{0.5}$ coating which is an appreciable improvement on the hardness of the mild steel baseplate which is about 155.3 ± 1.01 $HV_{0.3}$.
3. It was observed that the wear rate decreased linearly as Nb addition was increased, indicating that the addition plays an important role in improving the coating's wear resistance. A wear rate of the order $\times 10^{-5}$ mm^3/Nm was recorded from 0.75 Nb and above, which is an appreciable improvement over wear rates of the order $\times 10^{-4}$ mm^3/Nm that were seen in the mild steel baseplate and CrCoNiCu alloy. The improved wear resistance was imparted by plastically deformed Cu-rich thin oxide that was reinforced by Laves phases to form compacted protective tribo-layer.
4. Corrosion resistance varied with Nb addition. An optimum corrosion resistance of 0.0032 mm/year was recorded by $CrCoNiCuNb_{0.25}$ coating, which is more than a 260-fold improvement when compared to the steel baseplate in 3.5% NaCl electrolyte.

In summary, the goal of adding varied content of Nb to CrCoNiCu to achieve coatings with improved hardness values, wear and corrosion resistance was achieved. The coatings were deposited on a mild steel substrate and optimum hardness value was recorded at 0.5 Nb addition, lowest wear rate was observed at 0.75 Nb content and 0.25 Nb addition resulted in a coating with the best corrosion resistance in 3.5% NaCl solution. The considerable improvements observed in the properties studied showed that the coatings can be used to extend the applicability and enhance the service life of mild steel in heavy duty machine parts use for tillage and excavation.

References

1. W. R. Gill and G. E. V. Berg, Soil dynamics in tillage and traction. (ARS, USDA, 1967).
2. W. N. Bollinger, Earth excavation and transporting appliances, (1911).
3. K. Strafford and P. Datta, Surface Engineering (Routledge, 2018).
4. H. Aljibori, A. Alamiery, and A. Kadhum, Int. J. Corros. Scale Inhib. **12**, 1476-1520 (2023).
5. X. Ji, K. Guan, Y. Bao, Z. Mao, F. Wang, and H. Dai, Lubricants. **12**, 5 (2023).
6. W. Zhang, P. K. Liaw, and Y. Zhang, Sci. China Mater. **61**, 2-22 (2018).
7. D. E. Jodi and N. Park, *Mater. Lett.* **255**, 126528 (2019).
8. Y. Xie, Z. Xia, J. Hou, J. Xu, P. Chen, and L. Wan, Acta Metall. Sin. **34**, 1591-1600 (2021).
9. Y. Ren, Q. Jia, Y. Du, Q. Zhou, C. Greiner, K. Hua, H. Wang, and J. Wang, Friction. **10**, 1722 - 1738 (2022).
10. Y. Xie, X. Meng, Y. Chang, D. Mao, Y. Yang, Y. Xu, L. Wan and Y. Huang, Compos. Sci. Technol. **219**, 109225 (2022).

11. X. Xian, L. Lin, Z. Zhong, C. Zhang, C. Chen, K. Song, J. Cheng, Y. Wu, Mater. Sci. Eng. **713**, 134-140 (2018).
12. B. R. Gelchinski, I. A. Balyakin, A. A. Yuryev, and A. A. Rempel, Russ. Chem. Rev. **91**, 5023 (2022).
13. R. Bhaskaran Nair, R. Supekar, S. Morteza Javid, W. Wang, Y. Zou, A. McDonald, J. Mostaghimi and P. Stoyanov, Metals. **13**, 579 (2023).
14. C.H. Tsau, C.Y. Yeh, and M.C. Tsai, Mater. **12**, 3716 (2019).
15. F. He, Z. Wang, P. Cheng, Q. Wang, J. Li, Y. Dang, J. Wang and C.T. Liu, J. Alloys Compd. **656**, 284-289 (2016).
16. Y. Cai, Y. Chen, Z. Luo, F. Gao, and L. Li, *Mater. Des.***133**, 91-108 (2017).
17. W. Lu, X. Luo, Y. Yang, and B. Huang, *Mater. Express.* **9**, 291-298 (2019).
18. P. S. Deshmukh, S. Yadav, G. D. Sathiaraj, and C. Paul, Mater. Today Commun. **35**, 106351(2023).
19. H. Jiang, L. Jiang, D. Qiao, Y. Lu, T. Wang, Z. Cao, and T. Li, J. Mater. Sci. Technol. **33**, 712-717 (2017).
20. J. Wu, Y. Chen, and H. Zhu, *Adv. Eng. Mater.,* 24, 2101548 (2022).
21. Luo, D., Zhou, Q., Huang, Z., Li, Y., Liu, Y., Li, Q., He, Y. and Wang, H., Coatings, **12**, 1428 (2022).
22. L. Meijun, L. Xu, C. Zhu, Z. Li, and S. Wei, J. Mater. Res. Technol. (2023).
23. H. Ezatpour and M. Torabi-Parizi, J. Mater. Res. Technol. **29**, 5447-5463 (2024).
24. H. Liang, H. Yao, D. Qiao, S. Nie, Y. Lu, D. Deng, Z. Cao and T. Wang, J. Therm. Spray Technol. **28**, 1318-1329 (2019).
25. X. Shi, G. Li, M. Zhang, H. Xu, and Z. Li, J. Alloys Compd. **960**, 170905 (2023).